# Observational analysis of the daily cycle of the planetary boundary layer in the central amazon during a typical year and under the influence of the ENSO (GoAmazon project 2014/5)

Rayonil G. Carneiro[1], Gilberto Fisch[2]

[1] National Institute for Space Research (INPE), Sao José dos Campos, Brazil
[2] Department of Aerospace Science and Technology, São José dos Campos, Brazil

*Correspondence to*: Rayonil G. Carneiro (rayonilcarneiro@gmail.com)

**Abstract** The Amazon biome contains more than half of the remaining tropical forests of the planet and has a strong impact on aspects of meteorology such as the Planetary Boundary Layer (PBL). In this context, the objective of this study was to conduct observational evaluations of the daily cycle of the height of the PLB during its stable (night) and convective (day) phases from data that were measured and/or estimated using instruments such as a radiosonde, SODAR, ceilometer, wind profiler, Lidar and microwave radiometer installed in the central Amazon during 2014 (considered a typical year) and 2015 during which an intense El Niño Southern Oscillation (ENSO) event predominated during the GOAmazon experiment. The results from the four intense observation periods (IOPs) show that during the day and night periods, independent of dry or rainy seasons, the ceilometer is the instrument that best describes the depth of the PBL when compared with *in situ* radiosonde measurements. Additionally, during the dry season in 2015, the ENSO substantially influenced the growth phase of the PBL, with a 15% increase in the rate compared to the same period in 2014.

## 1. Introduction

The Amazon basin covers about a third of the South American continent and extends for approximately $6.9 \times 10^6$ km$^2$, of which about 80% are covered by tropical forests (Tanaka et al., 2014; Ghate and Kollias, 2016). The Amazon biome represents more than half of the world's remaining tropical forests, and consequently has a strong impact on the climate of South America, thus is one of the major tropical convective regions in the global climate system (Tang et al., 2016). It provides moisture to the global hydrological cycle and energy to drive the global atmospheric circulation, with with a large influence on meteorological components such as the Planetary Boundary Layer (PBL). Understanding convective systems over the Amazon region through observations is important for understanding and simulating this systems.

In this region there is a substantial quantity of convective activity that occurs during the entire year, but there are significant seasonal differences due to annual variation of atmospheric circulation and thermodynamic structure (Marengo and Espinoza, 2016), and these wet (or rainy) and dry season are well-defined. In this context, during the years 2014 and 2015, in the central Amazon region, the *Green Ocean Amazon* (GOAmazon) project was conducted with the objective of observing the influence of the complex interaction between the pollution plume generated in the city of Manaus-Amazonas, and clouds and vegetation (Martin et al., 2016). This project approached research questions from a multidisciplinary perspective, and one of the studied topics was the physics involved in convective processes in the Amazon with emphasis on differences between wet and dry seasons.

The PBL is a turbulent layer of the atmosphere near the surface that results from the interaction between the surface and the atmosphere. The knowledge of the properties of the PBL has important scientific and practical applications because through

38    this understanding of the PBL operational models of weather and climate forecasting can be refined, pollutant dispersion

39    processes can be adequately described, the eolic potential of a region can be objectively determined, patterns of ventilation in

40    urban areas can be estimated, and improvements in agricultural techniques can be made (Englberger and Dörnbrack, 2017).

41    Furthermore, a more realistic representation of processes that occur in the PBL can benefit numeric models of weather

42    forecasting with better parameterization of convection, clouds, and rain (Holtslag et al., 2013). The PBL characteristics,

43    related to surface processes, provide important information regarding the priming of the atmosphere for convective initiation

44    (Tawfik and Dirmeyer, 2014).

45    Holtslag et al. (2013) state that the PBL, since it is the lowest level of the atmosphere, is in continuous interaction with the

46    Earth's surface, with significant turbulent transfer of heat, mass, and *momentum*. According to these authors the PBL

47    presents, during its daily cycle, large variations in temperature, wind, and other variables in response to atmospheric

48    turbulence and convective processes that occur in a tridimensional and chaotic form in timescales that range from seconds to

49    hours, and the length across which these events occur are between a few millimeters up to the entire depth of the PBL (1-2

50    km) or more in the case of convective clouds.

51    Neves and Fisch (2015) emphasize that an important characteristic of the PBL is the determination of its height because it is

52    then possible to estimate the volume into which the source of pollution will be dispersed, and this is an important parameter

53    for modeling of atmospheric dispersion. During its daily cycle the PBL undergoes atmospheric processes generated by

54    thermal and mechanical convection during the day, and displays stable conditions at night. The height of the PBL during the

55    atmospheric instability phase (principally during the day) is denominated the Convective Boundary Layer (CBL), and that

56    during the stable period (principally at night) is named the Nocturnal Boundary Layer (NBL).

57    In this context, observational evaluation of the daily cycle of the PBL, with emphasis on the CBL and NBL, represents an

58    important field of study since within the PBL there occur processes that have large impact on society and the terrestrial

59    environment. Therefore, the objective of this study was to contribute to a more thorough understanding of the daily cycle of

60    the height of the PBL through integration and comparison of data that were measured and/or estimated using instruments

61    such as a radiosonde, SODAR, ceilometer, wind profiler, Lidar and microwave radiometer installed by the GOAmazon

62    experiment. Furthermore, this study attempted to verify if the observational methods were representative of the daily

63    variation in the cycle of the CBL and NBL in the central Amazon during 2014 (stated as a normal year) and 2015, and to

64    elucidate the influence of an intense El Niño Southern Oscillation (ENSO) event that occurred in 2015/2016.

65

## 2. Material and Methods

67    In order to conduct this observational study, data from the GOAmazon project 2014/5 were used. The article by Martin et al.

68    (2016) describes the details of the experiment wherein these data were collected, its principal objectives, and some results.

69    These data were collected using the structure that was installed at a research station called T3 (03º 12' 36" S; 60º 36' 00"

70    W), located north of the municipality of Manacapuru in the State of Amazonas, about 9.5 km from the urban area, and about

71    11.5 km from the left bank of the Solimões River, at the confluence of the mouth of the Manacapuru River (Figure 1) in the

72    central region of the Amazon basin.

73

74    At the experimental site of the T3 station, instruments were installed to obtain measurements of the hydrological cycle, PBL

75    energy flux, and other micrometeorological variables, and the data from these measurements are available on the site of

76    ARM - Climate Research Facility (https://www.arm.gov). For the current study, four intense observation periods (IOP) were

77    defined in order to capture the peak of the rainy (February and March) and dry (September and October) seasons of 2014 and

78    2015. The dates for each IOP were IOP1 and IOP3, February 15 to March 31, 2014 and 2015, and IOP2 and IOP4, from

79  September 1 to October 15, 2014 and 2015. For the daily cycle analysis of the PBL it was considered the sunrise at 06 LT

80  and the sunset at 18 LT, not varying throughout the year.

81  In order to measure the height of the PBL, remote sensing estimation methods including a Wind Profiler (WP), Ceilometer,

82  SODAR, Microwave Radiometer Profiler (MWP) and Lidar were used, and these data were compared to data taken *in situ*

83  obtained using radiosondes (RS), and this method is described below.

### 2.1 Radiosonde (*in situ*) –RS

85  In this experiment RS measurements were obtained using a system that included a DIGICORA (MW12) (Vaisala Inc.,

86  Finland) with radiosonde model RS92SVG. The RS were coupled to a meteorological balloon that had an average ascension

87  rate of 5 m s$^{-1}$, and the readings were taken at 02, 08, 14 and 20 Local Time (LT), and during the IOPs 1 and 2 and extra RS

88  was done at 11 LT to better characterize the convective phase. From the RS measurements other data were taken which

89  included pressure, altitude, geographic position (latitude and longitude), air temperature (dry bulb and dew point), relative

90  humidity, and wind velocity and direction. From these data the potential temperature ($\theta$) and specific humidity (q) were

91  extrapolated, and using the vertical profiles of $\theta$ and q the height of the PBL was calculated by identifying the vertical level

92  where there was a systematic increase in potential temperature and a sudden reduction in specific humidity, and this method

93  is called the two profile method, as described in detail by Santos and Fisch, (2007), Seidel et al., (2010) and Wang et al.

94  (2016).

### 2.2 Wind Profiler (WP)

96  In order to construct a wind profile (WP) at the study site, a Radio Acoustic Sound System (RASS) model RWP915 from

97  Vaisala Inc. (Finland) was used for direct and continuous measurements of the PBL. The WP are Doppler instruments used

98  to detect the vertical wind profile, and they function at a frequency of 50 MHz to 16 GHz. The WP/RASS installed at the

99  study site operates at 915 MHz to measure the wind profile. The RASS transmitter aids in the measurement of the profiles of

100  the vertical temperature. The RWP/RASS operates through transmission of electromagnetic waves in the atmosphere and

101  measures the intensity and frequency of the backscatter of the waves, assuming that atmospheric dispersion elements are

102  moving with the average wind profile.

103  Since this is an instrument that operates at a high frequency and using smaller intervals of space between layers, it is

104  frequently used for tropospheric observations, especially for the PBL. The method used in this study is described by Wang et

105  al. (2016), wherein the height of the PBL was estimated using the vertical profile of electromagnetic refraction of RWP,

106  where the maximum of this index occurs in the upper part of the PBL.

### 2.3 SODAR

108  In the study area a Mini SODAR (Sound Detection and Ranging) (SCINTEC, Germany) was installed. This monostatic

109  equipment consists of an emission/receiving antenna with an area of 1.96 m$^2$, and functions at a power of 10 W and a

110  frequency of approximately 2 kHz. Using the SODAR profiles of wind velocity and direction were obtained at intervals of

111  30 min at a maximum height of 400 m.

112  Through remote sensor measurement by the SODAR the height of the PBL was calculated for its night phase (NBL) through

113  the determination of the maximum wind height (jet). This method was suggested by Neves and Fisch (2011) and showed

114  good results for the Amazon due to its operational limit (400 m) and taking into account that the NBL in the region has an

115  average depth of 100 to 300 m.

### 2.4 Ceilometer

117    The PBL was also monitored using a Ceilometer model CL31 from Vaisala Inc. (Finland). Ceilometers are a LIDAR remote

118    sensing instruments that register the intensity of optical backscattering at the near infrared wavelength through an emission

119    of a vertical pulse that is autonomously executed. The data generated yield the height of the cloud base, and using this data

120    the height of the PBL is estimated (Shukla et al., 2014; Carneiro et al., 2016). The ceilometer is a high-frequency instrument

121    with a sampling rate of 16 s and is a powerful tool for measuring the height of the PBL during its daily cycle (day and night

122    phases) to a high level of detail. The intensity of backscattering depends on the concentration of particles in the air, but also

123    depends on the reflexive properties of the atmosphere, which are related to it level of humidity. Therefore, this instrument is

124    useful for creating a tridimensional map of aerosols, air pollutants, and industrial and natural emissions of particles.

125    Ceilometers use a retrodiffusion laser to determine the coefficient of the attenuated portion, and the coefficients for aerosols

126    are obtained from these data, and subsequently the heights of the cloud base and the PBL are calculated.


127    **2.5 Microwave Radiometer Profiler (MWR)**

128    Data were also used from a Microwave Radiometer Profiler model MP3000A from Radiometrics Corp., Boulder, CO, USA.

129    This instrument provides vertical profiles of temperature, humidity, and liquid water content at a sampling rate of 60 s and

130    average values at intervals of approximately 5 minutes.

131    The profiles are deduced from measurements of radiance values of absolute microwaves (expressed as "brightness

132    temperature") obtained at 12 different frequencies at intervals of 22-30 and 51-59 GHz. This type of data is useful as input

133    into numerical models of weather forecasting which need high resolution profiles in continuous time. The data for the air

134    temperature profile from the MWR were combined with the vertical pressure profile from the RS sampling in order to

135    interpolate these to the entire daily cycle, this allowing for the calculation of the vertical field of temperature potential and

136    obtain the PBL height through the profile method.


137    **2.6 Lidar**

138    LIDAR was also used to estimate the height of the PBL using a LIDAR from Halo Photonics (United Kingdom), a single

139    autonomous instrument from the most recent line of products from this company for atmospheric remote sensing. These

140    systems are adequate for meteorological studies of the PBL and also for measurements of cloud cover, vertical wind profiles,

141    and air quality monitoring (Gouveia et al., 2017).

142    Lidar is an active remote sensing instrument that provides measurements of radial velocity and attenuated backscattering in

143    real time. The fundamentals of its operation are similar to those of radar in which pulses of energy are transmitted to the

144    atmosphere, the energy that is bounced back to the receiver is collected and measured as a resolved signal in time. Starting

145    with the interval of time between each exiting pulse and the retro-diffused signal, the distance to the disperser is inferred.

146    The radial velocity or of the line-of-sight of the dispersers is determined using the movement of the Doppler frequency of the

147    retro-diffused radiation. LIDAR uses a technique of heterodyne detection (method of extraction of coded information as a

148    phase modulation and/or the frequency of a wavelength) in which the return signal is mixed with a reference laser beam (a

149    local oscillator) of a known frequency. A computer within the instrument then processes the signal determining the Doppler

150    frequency change using the spectrum from the signal. The energy content of the Doppler spectrums can also be used to

151    determine attenuated backscattering.

152    Lidar operates in the near infrared wavelength and is sensitive to retro-diffusion of aerosols at the micrometer scale,

153    therefore it is capable of measuring wind speeds under clear sky conditions with a very high precision (normally 10 cm s$^{-1}$).

154    Lidar also possesses a superior capacity for hemispheric sweeping, thus permitting tridimensional mapping of turbulent

155    fluxes within the PBL. Using the variance of the vertical wind speed ($\sigma w^2$) provided by the Lidar, the method of Huang et al.

156    (2017) was employed, where the authors define the depth of the PBL as a layer in which $\sigma w^2$ exceeds a specific limit (0.1 m$^2$

157    s$^{-2}$).

158    Table 1 presents a synthesis of the instruments used in this study, the observation periods, and temporal and spatial
159    resolutions.
160
161    Determination of monthly rainfall for both study years was done using data taken with a disdrometer model Parsivel[2] (OTT
162    Hydromet GmbH, Germany), with a temporal resolution of 10 minutes. The eddy covariance system provides an estimate of
163    the net exchange of energy and mass between the terrestrial surface and the atmosphere. The estimated flux is given by a
164    scalar magnitude that is defined as the average of the product of the fluctuations of the vertical velocity and the concentration
165    that is being transported. In practice, this technique consists of taking observations of variables of the product at a high
166    frequency, and from this large number of samples of each variable the statistical covariation is calculated between them. In
167    this manner the system provides *in situ* measurements of turbulent fluxes of *momentum,* sensible and latent heat, and carbon
168    dioxide to the surface.
169    The measurements of radiation and soil heat flux were done every 30 minutes using the Surface Energy Balance System
170    (SEBS), which consists of measurements of solar and terrestrial radiation collected using radiometers, and the radiation
171    balance by a net radiometer. There was coupling of sensors measuring soil temperature and heat flux in this system.
172


173    **3. Results and Discussion**

174    Analysis of the meteorological variables revealed that accumulated precipitation was different between years (Figure 2). The
175    year 2014 was similar to the normal climatology (for the city of Manaus - data extracted from INMET, 2018) for the region
176    (2,300 mm), with a total of 2,451 mm. This high rate of rainfall can be understood as a response of the dynamic fluctuation
177    of the nearly permanent center of convection, associated with a high rate of local evapotranspiration, which contributed to
178    recycling of water vapor and rainfall (NobrE et al., 2009; Rocha et al., 2017). In contrast, the year 2015 registered a
179    significant reduction (approximately 30%) of the total rainfall in relation to the previous year, with a total accumulation of
180    1,764 mm, well below the normal climatological average. This reduction is associated with the occurrence of the El Niño
181    Southern Oscillation (ENSO) event of that year (ECMWF, 2017, Macedo and Fisch, 2018; Newman et al., 2018).
182
183    During 2014, monthly accumulated precipitation was always above 50 mm month$^{-1}$, and during representative months of
184    IOP1 (February and March, 2014) the total accumulated precipitation was 720 mm. However, during IOP2 (September and
185    October, 2014) the total accumulated precipitation was 185 mm, yielding a reduction of nearly 75% of accumulated
186    precipitation during IOP1. According to Ferreira et al. (2005), this difference between the rainy and dry seasons occurs
187    because rainfall distribution in the Amazon is very irregular, with high spatial and temporal variability. Marengo et al.
188    (2017) provide a more detailed explanation of this characteristic to central Amazonia and include the large-scale forcing role
189    in the description of rainfall during the rainy and dry seasons.
190    While 2015 had a large reduction in rainfall, during the months of the period of intense observation of the rainy season
191    (IOP3) the accumulated precipitation was 398 mm, representing a reduction of approximately 50% of the total accumulated
192    precipitation during the rainy season of 2014 (IOP1). During IOP4, the total accumulated precipitation was well below the
193    normal climatological value, as well as in comparison to the same period in 2014 (IOP2), with a total registered precipitation
194    of 68 mm, a reduction of approximately 65% compared to IOP2. This occurred due to the EN event being more intense
195    during these months (ECMWF, 2017; Newman et al., 2018). The ENSO event (2015/2016) was considered one of the most
196    intense of recent years, with an intensity similar to that which occurred during 1982/83 and 1997/98 (ECMWF, 2017).
197

198 **3.1. Typical year (2014)**

199

200 Daily cycles of 30-minute averages of the components of the balance of energy are presented in Figure 3 for the period IOP1

201 (Figure 3A) and IOP2 (Figure 3B) for 2014. In these figures, the radiation balance (Rn) had positive values between 06 and

202 18 LT, with 455W $m^{-2}$ for IOP1 at 12 LT, and IOP2 had greater intensity of Rn with 534.5 W $m^{-2}$ at 11 LT.

203 The latent heat flux (LE) showed that the majority of the available net radiation (daytime conditions) was used for this flux.

204 Both periods had similar maximum values, with 355.9 (IOP1) and 350 W $m^{-2}$ (IOP2) at 12 LT. However, there was a

205 reduction of net radiation converted into LE between the periods, with 75% in IOP1 and 66% in IOP2. This occurred

206 because IOP2 had lower availability of soil moisture for evapotranspirative processes.

207

208 In the Amazon, especially during the rainy season, only a small fraction of Rn (about 10%) is transformed into sensible heat

209 flux (H), and this maximum of 52 W $m^{-2}$ occurred at 10:30 LT during IOP1, while for IOP2, due to lower precipitation

210 values and soil moisture deficit, there was an increase of 21% of the fraction of Rn transformed into H, with a maximum of

211 112.8 W $m^{-2}$ at 12 LT.

212 Nevertheless, only a small percentage of Rn is converted into heat flux in the soil (G), with a maximum of 50 W $m^{-2}$ for both

213 IOPs. These results showed that independent of the season, this flux is always low, and is limited to about 5% of the total

214 available energy.

215 Figure 4 shows the hourly average of the heights of the PBL for the IOP1 (Figure 4A), and IOP2 (Figure 4B). Diurnal

216 (convective) and nocturnal (stable) conditions were separated by vertical lines at 06 and 18 LT, The RS (*in situ*

217 measurements) was considered as truth depth of the Boundary Layer, while the others presented estimated by remote

218 sensing.

219 During the phase in which the NBL is formed (between 00 and 06 LT), the IOP1 showed small vertical oscillations of its

220 depth due to the occurrence of sporadic rainfall (Figure 4A). The results obtained from the ceilometer between 00 and 03 LT

221 showed that the depth of the PBL varied between 180 and 280 m, and after 04 LT there was an increase in the maximum

222 height to 350 m, which was reduced in the following hours to 275 m by 06 LT (sunrise).

223 The measurements made with the WP also showed some oscillations in the height of the NBL, with a reduction in height

224 between 00 and 02 LT from 280 m to 250 m, and then an increase to a maximum of 350 m at 04 LT, remaining constant

225 until 06 LT. The SODAR results during this interval showed lower variation of NBL depth during this same interval. The

226 variation observed from the measurements by the different sensors is related to intermittent mechanical turbulence which

227 could be the result of the presence of clouds and rain during some days and not on others, thus provoking an increase in wind

228 variability during the night which has the effect of deepening the NBL. However, in this same interval during IOP2 (Figure

229 4B) the NBL was very stable with an average height of 250 m for all sensors (ceilometer, WP, SODAR, MWR and Lidar),

230 thus corroborating the explanation of the influence of rainfall on the determination of variability of depth of the NBL.

231 The results found for the height of the NBL were similar to those reported by Neves and Fisch (2011), in a study using

232 SODAR in southwestern Amazon, where the authors observed NBL heights varying from 150 to 329 m. However, Acevedo

233 et al. (2004), also studying in a pasture site in the Amazon (in Santarém-PA), observed lower NBL heights than those from

234 the current study (between 50 to 150 m), and this difference occurs because of different geographic conditions (Santarém

235 suffers the influence of river breeze). An example of the influence of the geographic factor is the fact that, in this case, in the

236 Santarém region the authors related several cases of formation of fog during the night, and this is one criteria that determines

237 the height of the NBL, but this phenomenon did not occur at the pasture site in Rondônia nor at T3 site in the current study.

238

Atmospheric
Chemistry
and Physics
Discussions

239   The phase of the erosion of the NBL begins at 06 LT when there is incidence of solar radiation after sunrise, but during IOP1
240   the most significant increase in Rn and consequently of H, occurred at 07 LT (Figure 3A). As a function of the small
241   increase in these fluxes during the first hours of the daytime period there is no increase in the PBL depth up to 08 LT,
242   indicating that the NBL that formed there was still not degraded. After 08 LT an increase in PBL height begins to be
243   registered, but only with an average rate of 22.8 m h$^{-1}$. This occurs due to a lower availability of energy in the IOP1, which
244   causes the erosion of the NBL to progress slowly, and total erosion occurs only at 09 LT when average rate is 102 m h$^{-1}$.
245   According to Stull (1988), the complete erosion of the NBL occurs when the PBL has a high growth rate (say above 100 m
246   h$^{-1}$).

247   In contrast, in the IOP2, as a function of greater stability of the NBL and the positive values of Rn and H occurring earlier,
248   initial erosion of the NBL begins at 06 LT and there is a rapid increase in the depth of the PBL compared to IOP1, and this
249   increase continues in the subsequent hours at a rapid rate of 70.8 m h$^{-1}$, which causes the NBL to be completely eroded by 08
250   LT. This result demonstrates that the erosion of the NBL in this region is conditioned by greater availability of energy in the
251   early hours of the morning, and by how much of this energy will be used for heating of the atmosphere (H).

252   In IOP1, after complete erosion of the NBL the development phase of the convective boundary layer (CBL) begins, and due
253   to the slow erosion of the NBL the growth of the CBL begins at 11 LT with a typical height of 850 m and an average
254   increase of 102 m h$^{-1}$, until it reaches its greatest depth at 1,180 m at 13 LT. However, soon after the maximum is registered,
255   the CBL presents a small reduction in depth (13.3 m h$^{-1}$), due to the low value of H, which did not exceed 50 W m$^{-2}$. This
256   surface flux, added to the entrainment flux at the top of CBL, was not sufficient to maintain turbulence in this layer, that
257   showed a reduction after this time.

258   During IOP2, with the NBL being rapidly degraded, the CBL that subsequently formed had a more rapid development, with
259   an average growth rate of 175.2 m h$^{-1}$. The CBL had a more prolonged phase, with maximum depth registered at 13:30 LT
260   of 1,590 m. After this maximum of the CBL there was a slight reduction in its growth rate (-39,2 m h$^{-1}$) until 17:30 LT,
261   when H returned to a null value. This depth is similar to that reported by Fisch et al. (2004), in a study of the CBL in a
262   pasture in Rondônia in the southwestern Amazon, where the authors observed a maximum depth in the dry season of 1,650
263   m. Neves and Fisch (2015) also observed in Rondônia that in the initial formation of the CBL during the dry season there
264   was very rapid growth between 08 and 11 LT, with maximum heights at 14 LT of about 1,500 m

265   **3.2. El Niño year (2015)**

266   The energy fluxes for IOPs 3 (Figure 5A) and IOP 4 (Figure 5B) show that during the 2015 rainy season, Rn IOP3 behaved
267   in an analogous manner as in the rainy season of 2014 (IOP1), with a maximum of 488 W m$^{-2}$ at 12 LT. However, during
268   the dry season of 2015 (IOP4) there was an increase in intensity compared to IOP2, with maximum Rn equal to 555.2 W m$^{-2}$ at
269   12 LT. This greater flux of net radiation to the surface will be converted into heat flux, meaning that there is greater energy
270   available during the dry season of 2015 compared to that of 2014 due to less cloud cover, a common characteristic in years
271   with ENSO events (Macedo and Fisch, 2018).
272
273   The LE registered a maximum of 310 W m$^{-2}$ during IOP3 at 12 LT. This result represented 65% of the partitioning of Rn.
274   These results are within the range of results for LE in this region, for which 70% of Rn is generally converted into LE (Von
275   Randow et al., 2004; Andrade et al., 2009). Due to the low the low water availability during IOP4 there was a reduction in
276   the partitioning of Rn into the LE flux, only about 35% in comparison with IOP3, resulting in a reduction of more than 50%.
277   The maximum LE registered was at 12 LT and was 179 W m$^{-2}$, while during IOP3 just 17% of Rn was converted into H,
278   with a maximum H observed at 13 LT of 86 W m$^{-2}$. During IOP4, H had larger averages and 60% of Rn was converted into

279    H, with a maximum of 280 W m$^{-2}$ at 12 LT. Furthermore, in 2015 during IOPs 3 and 4, only a small percentage of Rn was

280    converted into G, with a maximum of 40.0 W m$^{-2}$ in IOP3 and 50.0 W m$^{-2}$ in IOP4, both at 12 LT.

281    The daily cycle of CBL during IOP3 (Figure 6A), as well as in IOP1, showed vertical oscillations of the NBL´s heights

282    (between 00 and 06 LT), of 200 m (00:30 LT) to 375 m (03 LT). The WP and the SODAR yielded lower depths than did the

283    ceilometer and the MWR. However, during IOP4 (Figure 6B) the NBL was more stable, with an average height of 250 m,

284    similar to what was observed during IOP2. The result from 0 to 06 LT confirms that in the Amazon region the NBL is more

285    stable during the dry season compared to the rainy season, when it has larger variation in its depth.

286

287    The IOP3 demonstrated a similar erosion pattern for the NBL to that observed during IOP1, with the NBL still established

288    between 06 and 08 LT. From this time onward there was an increase in depth of the CBL with an average growth rate of 19.6

289    m h$^{-1}$. In this manner, just as in IOP1, the erosion of the NBL during IOP3 occurred slowly, with total degradation at 09 LT.

290    This result is similar to that which was observed during the same phase in IOP1, where the NBL was less stable, and together

291    with lower availability of energy at the surface, caused a slower erosion of the NBL. However, the erosion phase during

292    IOP4, in response to an increase in Rn and H, occurred earlier (06 LT). Additionally, during the dry season of 2015, the rate

293    of ascension was higher during the subsequent hours and reached 76.1 m h$^{-1}$, such that the NBL was completely eroded at 08

294    LT.

295    The development during IOP3 occurs in an analogous manner to that observed during IOP1, with weak vertical development

296    of the maximum depth. At 10 LT the CBL begins to develop and has a height of 830 m and a growth rate of 100.3 m h$^{-1}$,

297    reaching a maximum depth of 1,069 m (13:30 LT), demonstrating a shallower CBL during the wet season. However, in

298    contrast to IOP1, IOP3 had a CBL established during the entire evening period, probably as a function of lower frequency of

299    rainfall, and IOP4, during the 2015 dry season, had greater development of convection after erosion at 08 LT, with a high

300    growth rate of 193 m h$^{-1}$, and at 11 LT the CBL was completely established. With the CBL established as a result of greater

301    heating of the atmosphere by H, there was greater depth of the CBL, reaching a maximum of 1,925 m at 14 LT, and this was

302    influenced by the strong EN event, which intensified the dry season in the region, and has caused the highest values of H.

303    This caused greater thermal convection in the development of the CBL, which increased its depth by 21% in relation to that

304    observed in IOP2. This maximum depth of the CBL during IOP4 is not commonly found in studies conducted in the Amazon

305    region before, however Lyra et al. (2003), using radiosonde data, reported a maximum height of 2,200 m during the dry

306    season of 1994 in Rondônia.


307    **4. Conclusions**

308    During the four IOPS the results show that during daytime and nighttime intervals, independent of weather conditions, the

309    ceilometer is a promising sensor with good accuracy for direct and continuous measurement of the height of the PBL (which

310    on average ranged from 250 meters - NBL to 1,900 meters - CBL) when compared to *in situ* from RS. The RS, in spite of it

311    being a proven high-precision method, it did not capture the daytime evolution of the height of the PBL, due to the long time

312    interval between launches. While the MWR, WP and the Lidar were satisfactory for estimates of the convective phase (CBL)

313    of the PBL, during the nocturnal phase (NBL) these sensors overestimated heights. Additionally, the SODAR under- and

314    overestimated the NBL during these periods.

315    The intense EN event of 2015/2016 influenced the development phase of the CBL during the dry season of IOP4, and it had

316    a growth rate of about 15% higher than the results from IOP2, and a sensible heat flux (responsible for heating the air) that

317    was higher than the standard values for the central Amazon. As a consequence, more intense convective movements were

318    occurred and had contributed to a stronger vertical development of the layer.

Atmospheric
Chemistry
and Physics
Discussions

319  The NBL erosion showed differences between seasons, presenting an erosion time of 2 hours in the dry IOPs (2 and 4), and 3

320  hours in the wet IOPs (1 and 3). A more detailed analysis of CLN erosion is being elaborated in Carneiro and Fisch (2019).

321

322  **Data availability**. The data sets used in this publication are available at the ARM Climate Research Facility database for the

323  GoAmazon2014/5 experiment (https://www.arm.gov/research/campaigns/amf2014goamazon, last access: 1 June 2019).

324

325  **Author contributions**. RGC and GF designed the numerical experiments and the first author performed the simulations as a

326  part of his PhD. RGC performed data analysis, assisted by GF. RGC and GF prepared the manuscript.

327

328  **Competing interests**. The authors declare that they have no conflict of interest.

329

334

335  **References**

336  Acevedo, O. C., Moraes, O. L. L., Silva, R., Fitzjarrald, D. R., Sakai, R. K., Staebler, R. M., and Czikowsky, M. J. Inferring

337  nocturnal surface fluxes from vertical profiles of scalars in an Amazon pasture. **Global Change Biology**. 10, 886–894, doi:

338  10.1111/j.1529-8817.2003.00755.x, 2004.

339

340  Andreae, M. O., Acevedo, O. C., Araùjo, A., Artaxo, P., Barbosa, C. G. G., Barbosa, H. M. J., Brito, J., Carbone, S., Chi, X.,

341  Cintra, B. B. L., Silva, N. F. da, Dias, N. L., Dias-Júnior, C. Q., Ditas, F., Ditz, et al. The Amazon Tall Tower Observatory

342  (ATTO): overview of pilot measurements on ecosystem ecology, meteorology, trace gases, and aerosols. Atmospheric

343  Chemistry and Physics. 15, 10723–10776, doi: 10.5194/acp-15-10723-2015, 2015.

344

345  Carneiro, R. G., Fisch, G., and Kaufmann, T. Determination of Planetary Boundary Layer heights in the Forest Amazon

346  Using a Ceilometer. **Ciência e Natura**. 38, 460–466, doi: 10.5902/2179460X20309, 2016.

347

348  Carneiro, R. G., and Fisch, G. Analyze NBL erosion in the the Amazonia using large eddy simulation model. Manuscript

349  submitted for publication.

350  If an article is available via the internet, an URL address can be inserted before the year, e.g. "available at:

351  https://www.copernicus.org/, 2018".

352  ECMWF. The 2015/2016 El Nino and beyond. ECMWF Newsletter. Available at:

353  https://www.ecmwf.int/en/newsletter/151/meteorology/2015-2016-el-nino-and-beyond, 2017. Access in: 20 de may 2019.

354

355     Englberger, A., and Dörnbrack, A. Impact of Neutral Boundary-Layer Turbulence on Wind-Turbine Wakes: A Numerical
356     Modelling Study. **Boundary-Layer Meteorology**. 162, 427–449, doi: DOI 10.1007/s10546-016-0208-z, 2017.

357

358     Ferreira, S. J. F., Luizão, F. J., and Dallarosa, R. L. G. Internal rainfall and rainfall interception in dryland forest subjected to
359     selective logging in Central Amazonia. Acta Amazônica. 35, 55–62, doi: 10.1590/S0044-59672005000100009, 2005.

360

361     Fisch, G., Tota, J., Machado, L. A. T., Dias, M. A. F. S., Lyra, R. F. d. F., Nobre, C. A., Dolman, A. J., and Gash, J. H. C.
362     The convective boundary layer over pasture and forest in Amazonia. Theoretical and Applied Climatology. 78, 47–59, doi:
363     10.1007/s00704-004-0043-x, 2004.

364

365     Ghate, V. P., and Kollias, P. On the controls of daytime precipitation in the Amazonian dry season. **Journal of**
366     **Hydrometeorology**. 17, 3079–3097, doi: 10.1175/JHM-D-16-0101.1, 2016.

367

368     Gouveia, D. A., Barja, B., Barbosa, H. M. J., Seifert, P., Baars, H., Pauliquevis, T., Artaxo, P. Optical and geometrical
369     properties of cirrus clouds in Amazonia derived from 1 year of ground-based lidar measurements. **Atmospheric Chemistry**
370     **and Physics**. 17, 3619–3636, doi: doi:10.5194/acp-17-3619-2017, 2017.

371

372     Holtslag, A. A. M., Svensson, G., Baas, P., Basu, S., Beare, B., Beljaars, A. C. M., Bosveld, F. C., Cuxart, J., Lindvall, J.,
373     Steeneveld, G. J., Tjernström, M. Stable atmospheric boundary layers and diurnal cycles—challenges for weather and
374     climate models. **Bulletin of the American Meteorological Society**. 94, 1991–1706, doi: 10.1175/BAMS-D-11-00187.1,
375     2013.

376

377     Huang, M., Gao, Z., Miao, S., Chen, F., Lemone, M. A., Li, J., Hu, F., and Wang, L. Estimate of Boundary-Layer Depth
378     Over Beijing, China, Using Doppler Lidar Data During SURF-2015. **Boundary-Layer Meteorology**. 162, 503–522, doi:
379     DOI 10.1007/s10546-016-0205-2, 2017.

380

381     Lyra, R. F. d. F., Molion, L. C. B., Silva, M. R. G. D., Fisch, G., and Nobre, C. A. Some aspects of the atmospheric
382     boundary layer over western Amazonia: Dry Season 1994. **Revista Brasileira de Meteorologia**. 18, 79–85, 2003.

383

384     Macedo, A. S., and Fisch, G. Temporal variability of solar radiation during the GOAmazon 2014/15 experiment. Revista
385     Brasileira de Meteorologia. 33, 353–365, doi: 10.1590/0102-7786332017, 2018.

386

387     Marengo, J. A., and Espinoza, J. C. Extreme seasonal droughts and floods in Amazonia: Causes, trends and impacts.
388     **International Journal of Climatology**. 36, 1033–1050, doi: 10.1002/joc.4420, 2016.

389

Marengo, J. A., FIsch, G., Alves, L. M., Souza, N. V., Fu, R., and Zhuang, Y. Meteorological context of the onset and end of
the rainy season in Central Amazonia during the GoAmazon2014/5. Atmospheric Chemistry and Physics. 17, 7671–7681,
doi: 10.5194/acp-17-7671-2017, 2017.

393

Martin, S., Artaxo, P., Machado, L. A. T., Manzi, A. O., Souza, R. A. F., Schumacher, C., Wang, J., Andreae, M. O.,
Barbosa, H. M. J., Fan, J., Fisch, G., Goldstein, A. H., Guenther, A., Jimenez, J. L., Poschl U., Silva Dias, M. A., Smith, J.
N., and Wendisch, M. Introduction: Observations and Modeling of the Green Ocean Amazon (GoAmazon 2014/5).
**Atmospheric Chemistry Physics**. 16, 4785–4797, doi: 10.5194/acp-16-4785-2016, 2016.

398

Neves, T. T. A. T., and Fisch, G. Nocturnal boundary layer on pastureland in Amazonia. **Revista Brasileira de
Meteorologia**. 26, 619–628, doi: 10.1590/S0102-77862011000400011, 2011.

401

Neves, T. T. A. T., and Fisch, G. The Daily Cycle of the Atmospheric Boundary Layer Heights over Pasture Site in
Amazonia. **American Journal of Environmental Engineering**. 05, 39–44, doi: 10.5923/s.ajee.201501.06, 2015.

404

Newman, M., Wittenberg, T., Cheng, L., Compo, G. P., and Smith, C. A. The extreme 2015/16 el niño, in the context of
historical climate variability and change. Bullet n of the American Meteorological Society. 99, 16–20, doi: 10.1175/BAMS-
D-17-0116.1, 2018.

408

Nobre, C., Obregón, G., Marengo, J., Fu, R., Poveda, G. Characteristics of Amazonian climate: Main features. In: Keller, M.,
Bustamante, M., Gash, J., Dias, P. S. (Ed.). Amazonia and global change. Geophysical Monograph American Ser.
Washington , DC: Geophysical Union Books. 186, 146–162, 2009.

412

Rocha, V. M., Correia, F. W. S., Teixeira da Silva, P. R., Gomes, W. B., Vergasta, L. A., Moura, R. G., Trindade, M. S. P.,
Pedrosa, A. L., and Santos da Silva, J. J. Rainfall recycling in the Amazon basin: The role of moisture transport and surface
evapotranspiration. Revista Brasileira de Meteorologia. 32, 387–398, doi: 10.1590/0102-77863230006, 2017.

416

Santos, L. R., and Fisch, G. Intercomparison between four methods of estimating the height of the convective boundary layer
during the RACCI - LBA (2002) experiment in Rondônia - Amazonia. **Revista Brasileira de Meteorologia**. 22, 322–328,
doi: 10.1590/S0102-77862007000300005, 2007.

420

Seidel, D. J., Ao, C. O., and Li, K. Estimating climatological planetary boundary layer heights from radiosonde observations:
Comparison of methods and uncertainty analysis. **Journal of Geophysical Research**. 115, 1–15, doi:
10.1029/2009JD013680, 2010.

424

Atmospheric
Chemistry
and Physics
Discussions

425    Shukla, K. K., Phanikumar, D. V., Newsom, R. K., Kumar, K. N., Ratnam, M. V., Naja, M., and Singh, N. Estimation of the
426    mixing layer height over a high altitude site in Central Himalayan region by using Doppler Lidar. **Journal of Atmospheric**
427    **and Solar-Terrestrial Physics**. 109, 48–53, doi: 10.1016/j.jastp.2014.01.006, 2014.

428

429    Stull, R. (Eds.): An introduction to boundary layer meteorology. Kluwer Academic Publishers, USA, 1988.

430

431    Tanaka, L. M. d. S., Satyamurty, P., and Machado, L. A. T. Diurnal variation of precipitation in central Amazon Basin,
432    **International Journal of Climatology**. 34, 3574–3584, doi: 10.1002/joc.3929, 2014.

433

434    Tang, S., Xie, S., Zhang, Y., Zhang, M., Schumacher, C., Upton, H., Jensen, M. P., Johnson, K. L., Wang, M., Ahlgrimm,
435    M., Feng, Z., Minnis, P., and Thieman, M. Large-scale vertical velocity, diabatic heating and drying profiles associated with
436    seasonal and diurnal variations of convective systems observed in the GoAmazon2014/5 experiment. **Atmospheric**
437    **Chemistry and Physics**. 16, 14249-14264, doi:10.5194/acp-16-14249-2016, 2016.

438

439    Tawfik, A. B., Dirmeyer, P. A. A process-based framework for quantifying the atmospheric preconditioning of surface-
440    triggered convection. **Geophysical Research Letters**. 41, 173 – 178, doi: 10.1002/2013GL057984, 2014.

441

442    Von Randow, C., Manzi, A., Kruijt, B., Oliveira, P., Zanchi, F., Silva, R., Hodnett, M., Gash, J., Elbers, J., Aterloo, M.,
443    Cardoso, F., and Kabat, P. Comparative measurements and seasonal variations in energy and carbon exchange over forest
444    and pasture in South West Amazonia. Theoretical and Applied Climatology. 75, 1–22, doi: 10.1007/s00704-004-0041-z,
445    2004.

446

447    Wang, C., Shi, H., Jin, L., Chen, H., and Wen, H. Measuring boundary-layer height under clear and cloudy conditions using
448    three instruments. **Particuology**. 28, 15–21, doi: 10.1016/j.partic.2015.04.004, 2016.

449

450

**Table 1: Instrument parameters.**

| | RS | WP | SODAR | *Ceilometer* | MWR | *Lidar* |
|---|---|---|---|---|---|---|
| **Observation period** | Jan/2014 to Dec/2015 | Jan/2014 to Dec/2015 | Feb/2014 to Dec/2015 | Jan/2014 to Dec/2015 | Oct/2014 to Dec/2015 | Jan/2014 to Dec/2015 |
| **Variables observed** | Pressure; Temperature; Humidity; Wind speed and direction | Wind (u, v, w); Wind direction | Horizontal wind velocity (u,v); Wind direction; Vertical wind velocity (w); | Height of base of clouds; PBL height; Vertical visibility; | Temperature; Relative humidity; | Variation of vertical velocity ($\sigma_w^2$); |
| **Vertical resolution (m)** | ~10 | 60 | 10 | -X- | ~100 | 30 |
| **Temporal resolution** | 4 to 5 times/day | 1 hour | 30 min | 16 s | 60 s | 10 min |

Figure 1: Location of the atmospheric measurement experiments in Manacapuru, Amazonas, Brazil.
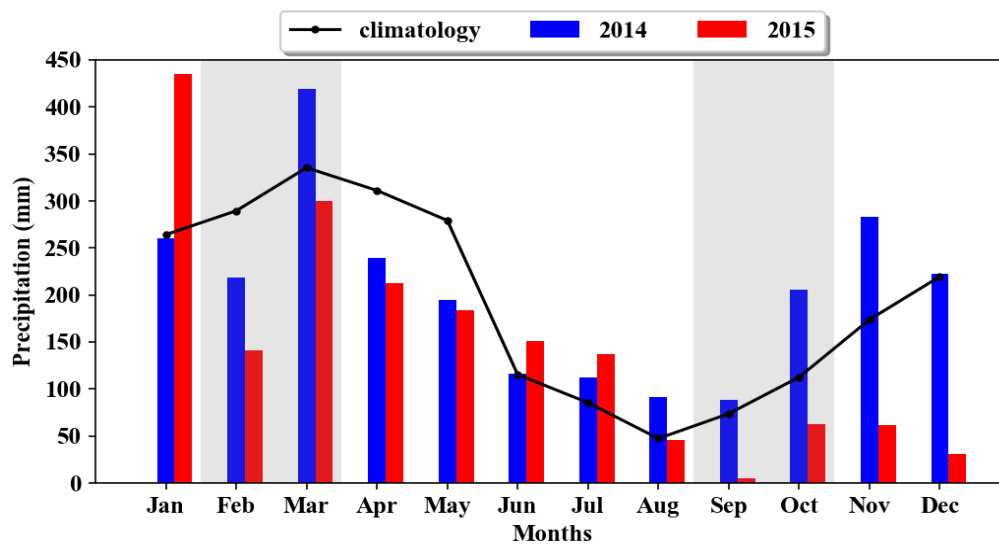


Figure 2: Distribution of accumulated monthly precipitation (mm) for the years 2014, 2015, and the normal climatological pattern.
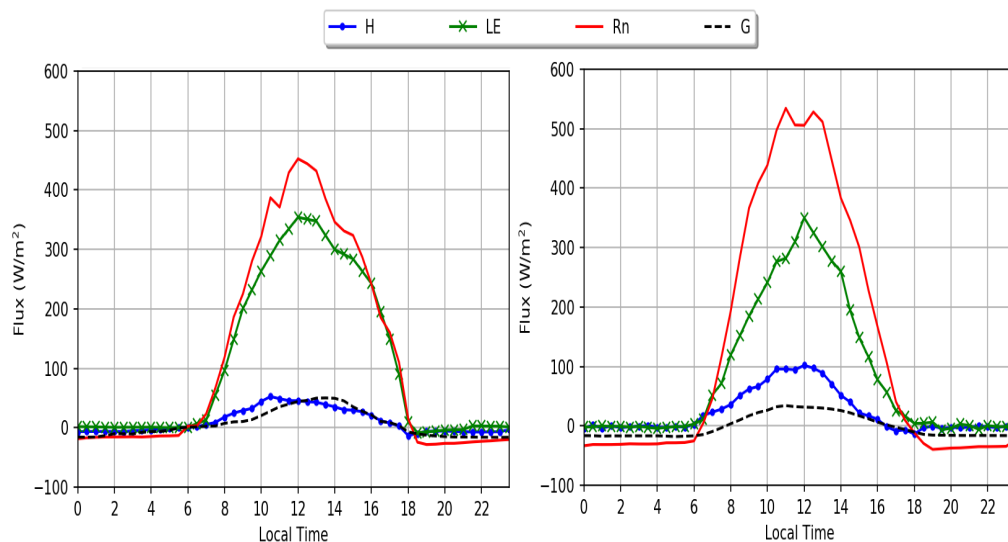
Figure 3: Average daily cycle of the radiation balance (Rn) (W m$^{-2}$), sensible heat flux (H) (W m$^{-2}$), latent heat flux (LE) (W m$^{-2}$) and soil heat flux (G) (W m$^{-2}$) during the IOPs 1 and 2.
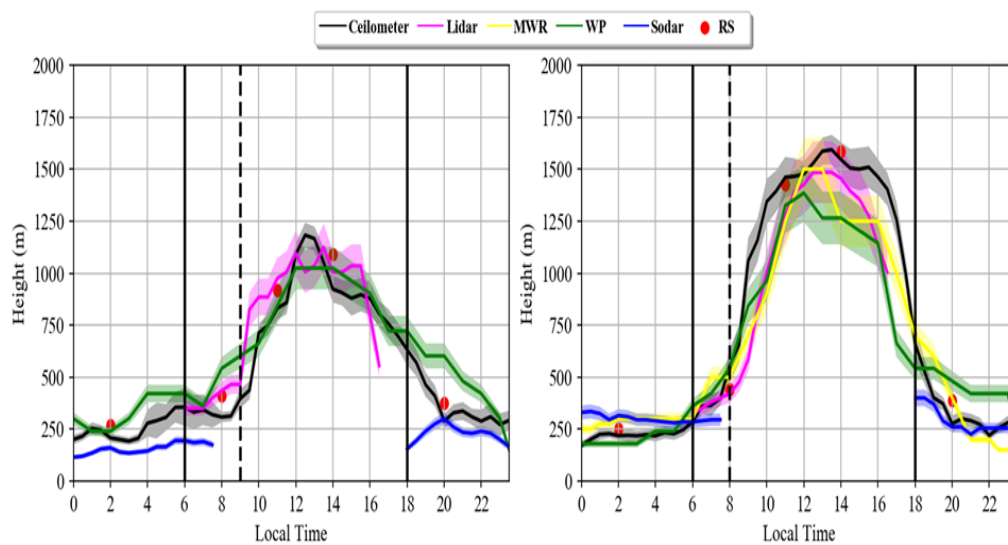


Figure 4: Daily cycle of the height of the PBL during IOP1 (A) and IOP2 (B) experimental periods. The vertical lines represent sunrise (06 LT) and sunset (18 LT).
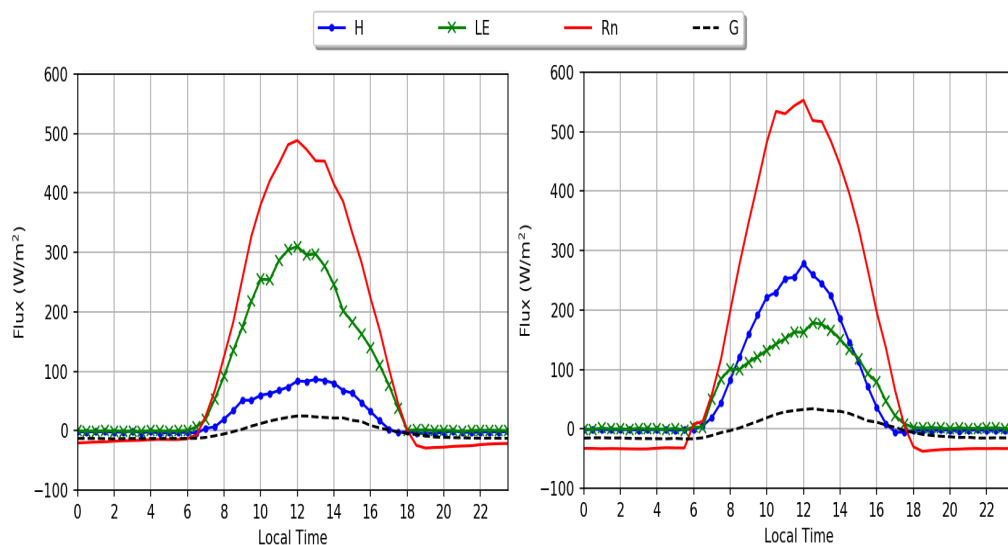
**Figure 5: Average of the daily cycle of net radiation (Rn) (W m⁻²), sensible heat flux (H) (W m⁻²), latent heat flux (LE) (W m⁻²) and soil heat flux (G) (W m⁻²) in the study region during the IOPs 3 and 4.**
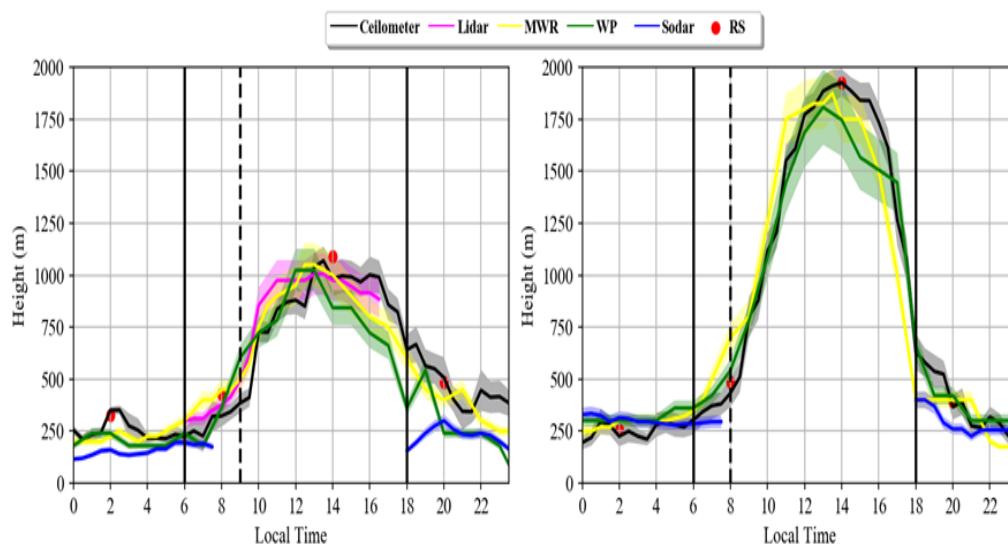


**Figure 6: Daily cycle of the height of the PBL during IOP3 (A) and IOP3 (B) experimental periods. The vertical lines represent sunrise (06 LT) and sunset (18 LT).**